RSC Advances

PAPER

View Article Online
View Journal | View Issue

Cite this: *RSC Adv.*, 2024, **14**, 24756

Lignin containing cellulose nanofiber/Ag_2Se nanocomposite films: a promising material for thermoelectric film generators

Ragab Abouzeid,*[ab] Mohammad Shayan,[a] Meen Sung Koo[a] and Qinglin Wu*[a]

Received 6th March 2024
Accepted 27th June 2024

DOI: 10.1039/d4ra01750a

rsc.li/rsc-advances

This work deals with the fabrication of lignin containing cellulose nanofiber (LCNF)/Ag_2Se films for thermoelectric applications. Ag_2Se nanoparticles were synthesized within the LCNF network through *in situ* methods, employing Na_2SeO_3 and $AgNO_3$ along with microwave energy treatment. LCNF/Ag_2Se films fabricated with two LCNF : Ag_2Se weight percent ratios (*i.e.*, 50 : 50 and 30 : 70) were used to construct a flexible thermoelectric module. The obtained Ag_2Se nanoparticles displayed a uniform size distribution in the LCNF network with smaller dimensions from the microwave energy treated group. The microstructure of LCNF/Ag_2Se films was improved by hot-pressing, leading to enhanced film density thermoelectric properties. At a differential temperature of 50 K, films with 50% and 70% of Ag_2Se exhibited output voltages of 18 and 21 mV; and Seebeck coefficients of −60 and −70 μV K^{-1} at 350 K, respectively. When microwave energy was applied, the films at 50% and 70% Ag_2Se showed highest output voltages of 19 and 33 mV, respectively, and Seebeck coefficients of −63.3 and −110 μV K^{-1} at 350 K. The low-cost fabrication process associated with this module opens a pathway for applications such as energy harvesting.

1. Introduction

Extended use of portable, flexible, and wearable electronics, coupled with the growth of the Internet of Things (IoT), has led to the development of self-powered devices that can draw power from human body and the environment.[1,2] Traditional battery-powered electronics face limitations in their service lifetime, requiring frequent charging or replacement, which increases costs and environmental pollution. To overcome these challenges, thermoelectric generators (TEGs) offer a promising solution by converting human body heat or low-grade waste heat into electrical energy. TEGs have several advantages, including no moving parts, no noise, easy maintenance, and high reliability. Particularly, flexible thermoelectric generators (f-TEGs) have attracted interest due to their capacity to convert heat directly into electricity, rendering them appropriate for wearable electronics and IoT applications. These f-TEGs exhibit flexibility, long lifetimes, and noiseless operation. f-TEGs can be divided into two classes, depending on their mode of operation. The first is made up of bulk thermoelectric materials, which capitalize on an out-of-plane temperature difference to generate power. The second type is composed of f-TEFs, which use an in-plane temperature difference. Although the former may have a higher thermoelectric efficiency, their lack of flexibility limits their use in practical applications.[3,4] During the past years, much attention has been given to the study of flexible thermoelectric (TE) materials and composites. Flexible substrates can be used to create thin films of TE materials with high efficiency. Additionally, conductive polymers and composites made of polymers and conductive fillers have been developed for this purpose. Ag_2Se is an n-type semiconductor with a small band gap (ranging from 0.04 to 0.2 eV) and low intrinsic thermal conductivity.[5–7] Ag_2Se has become a common choice for fabricating room temperature, flexible thermoelectric generators (TEGs).[8] Recently, Ag_2Se has been studied as a TE material, however, its performance is limited due to its low electrical conductivity compared to Cu_2Se. As a result, various conductive fillers have been explored as composite materials to improve TE performance.[9–11] It has been suggested that the integration of carbon nanotubes (CNTs) into materials such as Bi_2Te_3, Ag_2Se and Cu_2S can help increase their thermoelectric (TE) performance by uncoupling their TE parameters.[12–14] K. Zhou *et al.* 2016 achieved the successful growth of Ag_2Se thermoelectric thin films on either (La, Sr) (Al, Ta) O_3 or glass substrates. This was accomplished at a relatively low temperature of 100 °C through pulsed laser deposition. The optimized deposition kinetics and the correlation between shockwave plasma expansion and thin film characteristics indicate the potential for fabricating in-plan thermoelectric micro-devices suitable for room temperature applications.[15] Ag_2Se and composites containing reduced graphene oxide (rGO) were fabricated and hot-

[a]*School of Renewable Natural Resources, Louisiana State University, AgCenter, Baton Rouge, Louisiana 70803, USA. E-mail: rabouzeid@agcenter.lsu.edu; wuqing@lsu.edu*
[b]*Cellulose and Paper Department, National Research Centre, 33 Bohouth St., Dokki, Giza 12622, Egypt*

press densified, displaying a change in phase from orthorhombic to cubic at temperatures ranging from 390–450 K. The resulting material had a thermal conductivity of 0.492 W m^{-1} K^{-1} and a thermoelectric figure of merit (*ZT*) of 0.39 at 363 K, suggesting its potential for utilization in thermoelectric generators.[16] Different studies demonstrate the potential of Ag_2Se-based films as flexible and efficient materials for thermoelectric energy harvesting applications.[17] The addition of Ga doping to Ag_2Se films further improves their thermoelectric properties and increases their durability when subjected to mechanical stress.[18] Z. Shen *et al.* 2022 explores the potential of cellulose nanofibril-based foams, demonstrating enhanced shape-stability, compatibility, and improved heat transfer performance by incorporating multiwalled carbon nanotubes. The investigation focuses on their application in innovative sandwich structures of organic phase change materials with a thermoelectric generator for efficient solar energy harvesting and utilization.[19] D. Palaporn *et al.* (2022) have advanced the field by developing a highly efficient and flexible thermoelectric paper using bacterial cellulose/silver selenide nanocomposites, showcasing impressive properties, including a high-power factor and scalability, rendering it a promising candidate for practical applications in flexible thermoelectric generators.[20] Crispin *et al.*, demonstrated the potential of nanofibrillated cellulose (NFC) and poly(sodium-4-styrene sulfonate) (PSSNa) in TE applications. Their approach, which combined NFC with PSSNa to achieve a TE paper with notable mechanical flexibility and a competitive *ZT* value under high humidity conditions, underscores the importance of innovative material combinations.[21] The utilization of lignin containing cellulose nanofiber (LCNF), a sustainable and versatile material derived from biomass.[22–24] LCNF, known for its excellent mechanical properties and biodegradability, plays a pivotal role in the development of advanced composites for various applications, including thermoelectric devices.[25–28] The unique structural attributes of LCNF, such as its high surface area and the ability to form stable percolating networks, make it a suitable substrate for the synthesis of nanocomposites. The high surface area of LCNF provides numerous active sites for interaction and bonding with other materials, enhancing the performance of composite. Additionally, the ability of LCNF to form stable percolating networks contributes to improved mechanical strength and structural integrity. The presence of lignin not only reinforces the nanofiber network but also introduces functional groups such as phenolic, carboxylic, and aliphatic hydroxyl groups, which enhance the surface chemistry and reactivity of the nanofibers.[29] These functional groups facilitate the formation of strong bonds with various nanoparticles and polymers, leading to the development of composites with superior properties. Moreover, lignin imparts thermal stability to the nanofibers, making LCNF-based composites more suitable for high-temperature applications. These attributes collectively enhance the versatility and effectiveness of LCNF in various applications, ranging from flexible electronics to energy storage and conversion devices.[30,31] The mechanism for generating electrical energy in LCNF/Ag_2Se material is primarily based on the Seebeck effect, where a temperature difference between the hot and cold ends of the material induces a voltage. This occurs due to the movement of charge carriers, typically electrons and holes, from the hot side to the cold side, creating an electric potential. Additionally, in thermoelectric cells, this process can involve utilizing redox couples to induce oxidation–reduction reactions at the hot/cold ends, leading to the transfer of electrons. For ionic thermoelectric capacitors, the mechanism is based on the Soret effect, where the difference in migration rates of ions under a thermal gradient creates an electric potential difference.[32–34] Our work highlights the potential of using LCNF, combined with Ag_2Se, to enhance the performance of thermoelectric devices. This research focuses on developing thermoelectric materials that are cost-effective, flexible, and highly efficient for use in wearable and bendable electronic devices. The novel approach utilized microwave technology to facilitate the formation of Ag_2Se nanoparticles on the surface of the LCNF, allowing for the LCNF/Ag_2Se films. These films showed excellent flexibility and conformity to various shapes, making them suitable for use in wearable and flexible electronics.

2. Experimental

2.1. Materials

Silver nitrate ($AgNO_3$) (99.8%) and ascorbic acid (90% each) were obtained from ACI Labscan. The sodium selenite (Na_2SeO_3, 99.5%) was obtained from KemAus. Without any further purification, all chemicals were used as received.

2.2. Preparation of lignin containing cellulose nanofiber (LCNF)

To prepare LCNF, unbleached softwood fiber was milled using a high-speed rotor grinder at 2 wt% consistency. The pulp was then ground for two hours in an ultrafine friction grinder (MKCA6-2, Masuko Sangyo, Kawaguchi, Japan) with a disk gap of −90 μm. Finally, the suspension was homogenized in a model M-110EH-30 microfluidics machine (Microfluidics Corp., Newton, MA, USA) two times at 208 MPa pressure.

2.3. Synthesis of LCNF/Ag_2Se nanocomposite film

The LCNF/Ag_2Se nanocomposite film was prepared through a two-step process. Initially, a 2% wt LCNF suspension was mixed with Na_2SeO_3 (*e.g.*, 18 mmol) to form a suspension, then 1.0% of ascorbic acid (related Na_2SeO_3) was added and continuously stirred slowly for 6 hours at 80 °C. The Se nanoparticles precipitated in the network structure of LCNF. The LCNF/Se obtained was soaked in $AgNO_3$ solution (*e.g.*, 36 mmol) for 48 hours to convert the metallic Se into Ag_2Se, resulting in a sample referred to as MA. Another approach to produce LCNF/Ag_2Se, involved blending a 2% wt. LCNF suspension with a mixture of Na_2SeO_3 and $AgNO_3$, followed by microwave irradiation at 500 W at 120 °C for 3 minutes, with a subsequent 5 minute treatment, leading to the creation of a sample named BM. For both AM and BM, the Ag_2Se content was adjusted to be 50% or 70% in comparison to the LCNF (*i.e.*, 50 : 50 and 30 : 70 of Ag_2Se : LCNF) giving rise to four distinct samples: A50, A70,

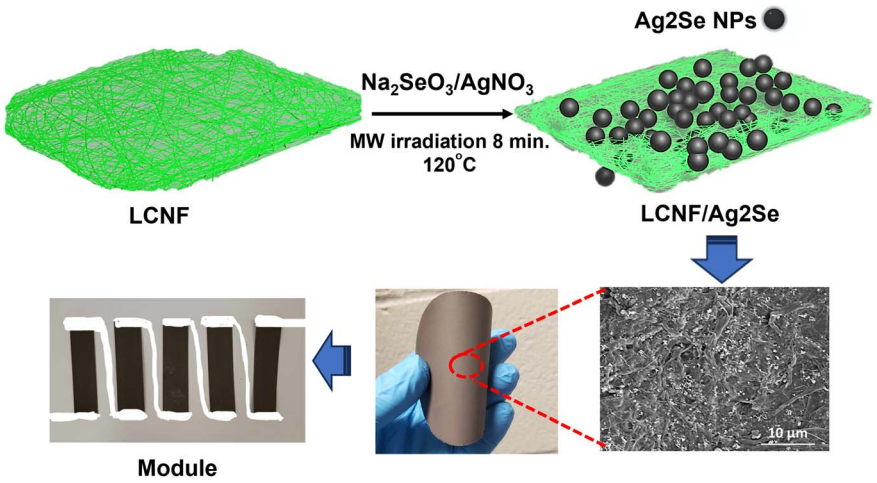

Fig. 1 The synthesis routes of LCNF/Ag_2Se.

B50, and B70. Finally, the nanocomposite films are fabricated through vacuum filtration and hot pressing (at 180 °C under a pressure of 1 MPa for 30 minutes), enhancing their density and thermoelectric performance. This detailed illustration (Fig. 1) underscores the importance of the synthesis process in optimizing the material structure and enhancing its applicability in flexible and wearable electronics.

2.4. Characterization of LCNF/Ag_2Se nano-paper

FTIR analyzer (Bruker Corporation, Billerica, MA, USA) in ATR mode was used to characterize the prepared LCNF/Ag_2Se. The X-ray diffraction was performed using a PANalytical Empyrean X-ray diffractometer (Malvern Panalytical Ltd., Malvern, Worcestershire, UK), with a CuKα radiation source ($\lambda = 1.5406$ Å) and 2θ range from 4° to 80°. A Quanta 3D DualBeam FEG FIB-SEM (Field emission scanning electron microscopy) and a JEM 1400 Transmission Electron Microscope (Peabody, MA, USA) were used to analyze the morphology of the LCNF and LCNF/Ag_2Se samples. The stress–strain curves of the LCNF/Ag_2Se nano-paper samples were obtained using a rheometer (AR 2000 ex, TA Instruments, Newcastle USA) in tensile mode and Young's modulus, were analyzed from the resulting data. Thermal gravimetric analysis (TGA) of LCNF and LCNF/Ag_2Se films was conducted in a nitrogen atmosphere with a Q50 Analyzer (TA Instruments Inc., New Castle, DE) at 30–60 °C with 10 °C heating rates. The absorbance of Ag_2Se solutions was measured at 300 to 700 nm, utilizing an Evolution™ 350 UV-visible spectrophotometer (Thermo Fisher Scientific Inc., Waltham, MA, USA).

2.5. Thermoelectric measurements

Strips of LCNF/Ag_2Se films were cut (40 mm × 5 mm) and then adhered to a substrate. Subsequently, the strips were interconnected in a series using an Ag paste as a conductive connection to create a prototype power generator. The output voltage, Seebeck coefficient (S) were recorded using an electrochemical workstation (CHI650E B14109, Chen Hua, China).

3. Results and discussion

3.1. FTIR, XRD and TGA analysis

The structural analysis of LCNF/Ag_2Se films depicted in Fig. 2 demonstrates the influence of microwave energy on the material properties. FT-IR patterns of LCNF and LCNF/Ag_2Se samples A50, A70, B50 and B70 are shown in Fig. 2a. All spectra exhibited an intense broad band at 3350 cm^{-1}, which is attributed to O–H stretching vibration in LCNF. The asymmetrical stretching of the C–H band was detected at 2930 cm^{-1}, with the band at 1643 cm^{-1} likely corresponding to water adsorption in the amorphous region of LCNF. The band at 1415 cm^{-1} was assigned to both CH_2 bending and C–O–O stretch. Spectra of A50, A70, B50 and B70 showed notable transmission peaks at 1552 and 1280 cm^{-1}, suggesting the presence of Ag–Se bonds in the nanoparticle structure of Ag_2Se. Fig. 2b shows the XRD patterns of prepared samples LCNF, A70 and B70. As previously reported,[35] samples A70 and B70 exhibit sharp and intense peaks of the orthorhombic Ag_2Se phase (P2221E), with characteristic (002), (112), (121), (103), (031), (200), (213), and (134). The XRD pattern indicates that there is a small number of secondary phases, such as Se and Ag_2SeO_3 (or Ag_2SeO_4). When microwave assisted preparation of LCNF/Ag_2Se is used, the intensity of the crystalline peak of LCNF is decreased for B70. The XRD curves were used to evaluate the crystallite size of Ag_2Se samples using the Scherrer equation.[16]

$$\text{Crystallite size } D(hkl) = \frac{K\lambda}{2B\cos\theta(hkl)} \quad (1)$$

where K is the shape factor, X-ray wavelength of the X-ray beam (λ), full width at half-maximum (FWHM) of XRD peak (B), and XRD peak position ($\theta(hkl)$) were all taken into consideration. The crystallite size was measured to be 26.24, 27.68, 20.56, and 22.71 nm for the samples A50, A70, B50 and B70 respectively. So, the use of microwave energy in the preparation of LCNF/Ag_2Se nanoparticles resulted in a reduction in crystallite size compared to samples prepared without microwave energy. Fig. 2 c illustrates the TGA weight percentage of the samples

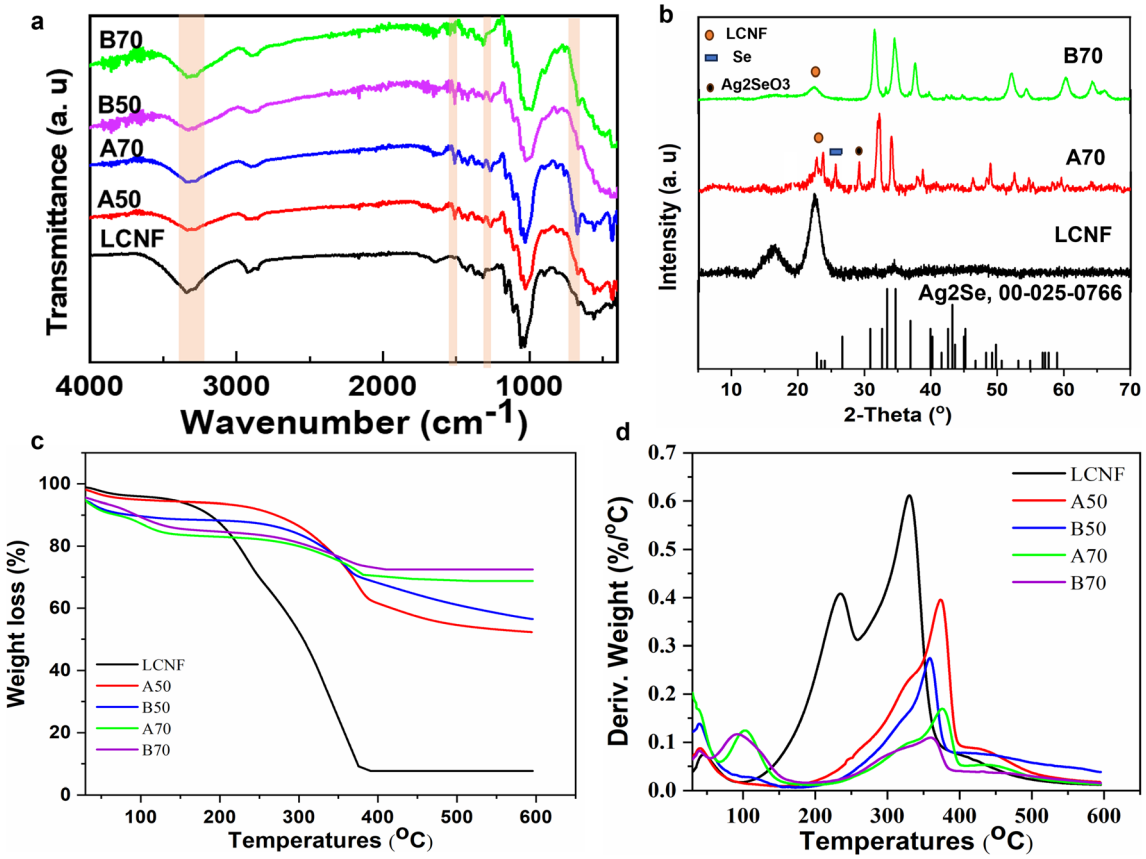

Fig. 2 Structural analysis of LCNF/Ag_2Se film (a) FTIR, (b) XRD, (c) TGA and (d) DTGA.

measured from 25 °C to 600 °C. A significant weight loss from 200 to 350 °C was observed for the pure LCNF sample, which is attributed to the decomposition of lignocellulosic materials. In comparison, the LCNF/Ag_2Se samples A50, A70, B50 and B70 showed higher thermal stability, with the major weight loss occurring from 300 to 450 °C. Subtract the residual weight of LCNF from the residual weight of LCNF/Ag_2Se samples at 600 °C in order to determine the amount of Ag_2Se in each sample. The wt% of Ag_2Se nanoparticles in A50, A70, B50 and B70 was found to be 44.7, 49.0, 60.2 and 64.9 wt%, respectively. The utilization of microwave energy as an assistant result in higher levels of Ag_2Se nanoparticles in LCNF. In Fig. 2d, DTGA curves derived from TGA measurements are shown. A large exothermic peak at ~300 °C was observed for the LCNF sample, indicating the decomposition of lignocellulosic materials. The LCNF/Ag_2Se samples A50, A70, B50 and B70 showed exothermic peaks ranging from 360 to 385 °C, which is associated with the phase transition from β-Ag_2Se to α-Ag_2Se.

3.2. Morphology structure of thermoelectrical generator

The thermoelectric (TE) phases of the LCNF/Ag_2Se are influenced by their morphology, as shown in Fig. 3. The SEM/EDX of both the LCNF (a) and LCNF/Ag_2Se (b–e) for samples A50, A70, B50 and B70 respectively and (f) after the hot-pressing (B50 as example). The LCNF network ensures that the Ag_2Se particles are uniformly distributed, with dimensions less than 500 nanometers and a narrow size distribution. The growth and clustering of Ag_2Se nanoparticles within the LCNF structure led to the formation of submicron sized Ag_2Se particles that are interspersed by the LCNF nanofibers. At the nanoscale, the microstructure produces interfaces that are able to hinder the transport of phonons by increasing the scattering of phonons across a variety of phonon wavelengths. After the hot-pressing process, Fig. 3f demonstrates that the LCNF/Ag_2Se film has a much-improved microstructure, with no visible voids and a dense surface. The only cracks are the result of laser beam exposure. The Ag_2Se nanoparticles were further characterized by elemental mapping, which showed that Ag and Se were homogeneously distributed. This suggests that Ag_2Se nanoparticles are within LCNF structure. This was further supported by elemental mapping and EDX analysis of the samples A50 and B50 Fig. 3(g, h) and (i, j) respectively which revealed strong signals from silver and Se atoms, a characteristic peaks of metallic silver and selenium nanoparticles. These results are consistent with previous reports of EDX spectra of Ag_2Se nanoparticles. Thus, the SEM analysis shows that the LCNF/Ag_2Se film has a good microstructure with no visible voids and a dense surface and the Ag_2Se nanoparticles are homogeneously distributed.

The TEM results of LCNF (Fig. 4a) indicated nanofibers that are interconnected, forming a network-like structure and some fibrils agglomerated into larger aggregate.[36–39] Sample A50 (Fig. 4b and c) contains Ag_2Se particles that are adhered to the LCNF network with slight aggregation, and the size of these particles is 26.0 ± 10 nm. On the other hand, sample B50

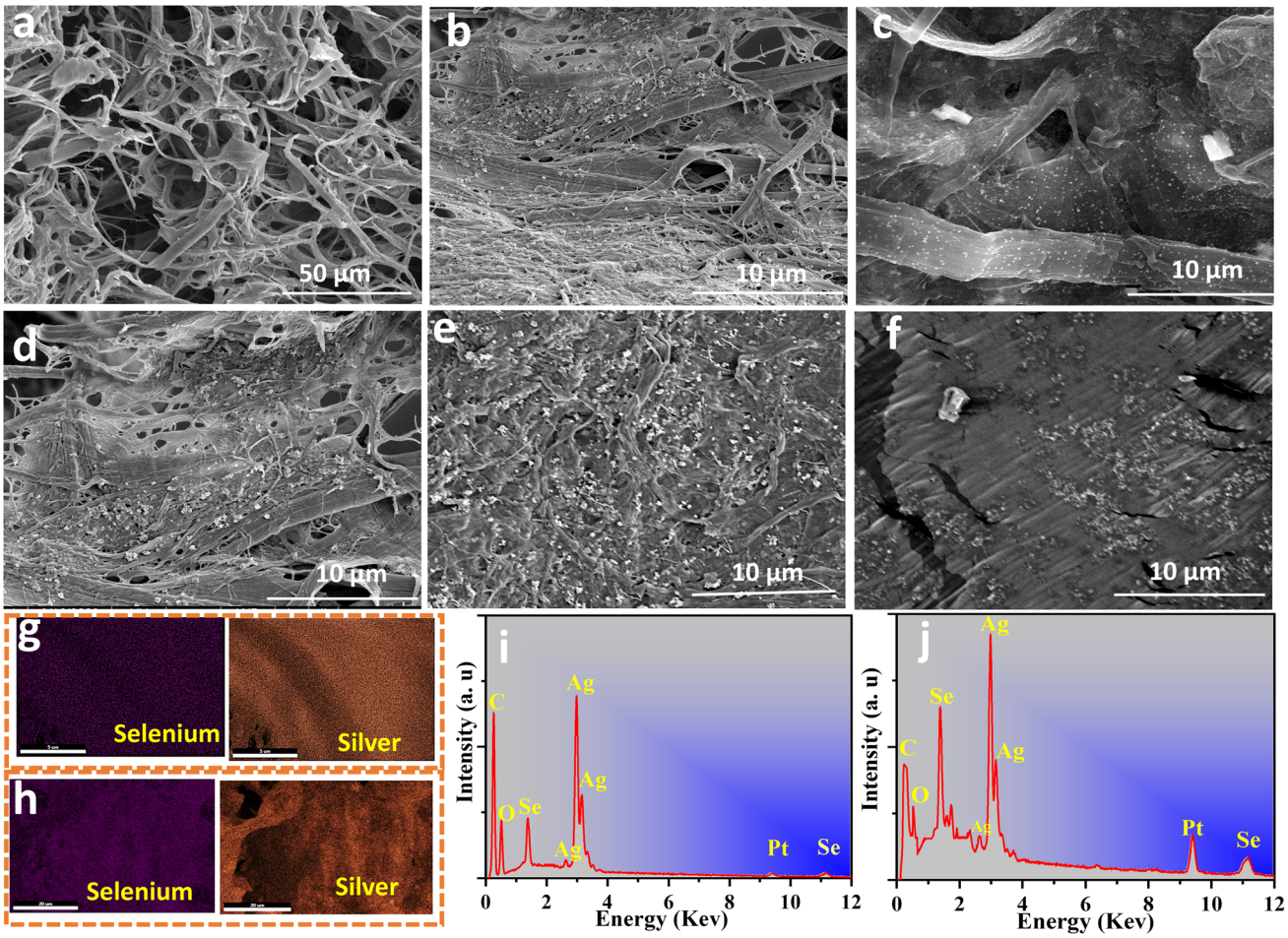

Fig. 3 Morphological analysis of LCNF/Ag_2Se films SEM of LCNF (a), LCNF/Ag_2Se (b and c) for A50, A70, and (d and e) for B50 and B70 respectively and (f) after the hot-pressing. Elemental mapping (g and h) and EDX spectra (i and j) for samples A50 and B50.

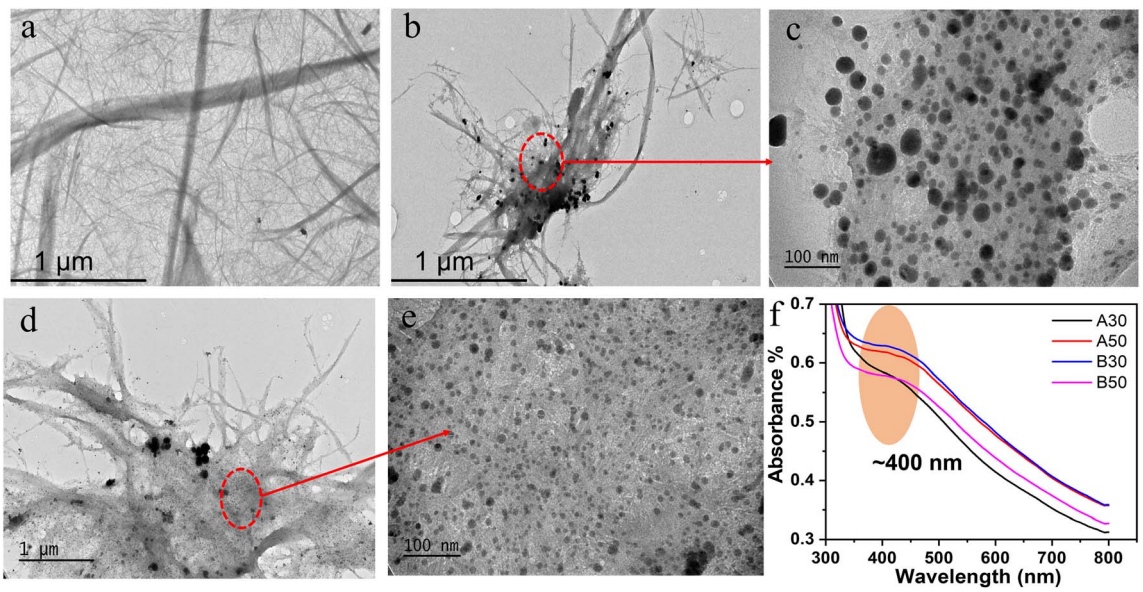

Fig. 4 (a) TEM images of LCNF, (b and c) LCNF/Ag_2Se (A50), (d and e) LCNF/Ag_2Se (B50) and (f) UV-vis spectra Ag_2Se samples.

(Fig. 3d and e) has Ag_2Se particles that are smaller, measuring 15 ± 2.4 nm, and are distributed homogenously without any agglomeration. This implies that, when LCNF/Ag_2Se is prepared without microwave energy assistant, the resulting Ag_2Se nanoparticles are larger than those produced using microwave energy assistant. Fig. 4f shows the UV-vis spectral analysis for samples A50, A70, B50 and B70, no distinct peaks corresponding to free silver or selenium nanoparticles were observed. Instead, the absorbance spectrum of Ag_2Se NPs was consistently detected at approximately 400 nm in all samples.

3.3. Chemical composition analysis

Fig. 5 represents the XPS results for chosen samples (A50 and B50) respectively. The survey scan of sample A50 and B50 illustrated revealed the presence of Ag and Se along with carbon and oxygen. The XPS spectrum results showed the presence of two Ag peaks with binding energies of 375 and 369 eV, which correspond to the doublet Ag $3d_{5/2}$ and Ag $3d_{3/2}$ of Ag^+. A separation energy of 6 eV between these two peaks demonstrated the character of the Ag^+ species. Additionally, peak was observed at 376.5.8 eV and 367.1 eV, indicating the presence of Ag–O–C bonds between LCNF network, thus confirming the presence of active hydroxyl groups on the LCNF surface. The Se 3d spectrum showed two peaks at 53.7 and 55.1 eV corresponding to Se $3d_{5/2}$ and Se $3d_{3/2}$ confirming that the chemical states of the elements in Ag_2Se NPs are Ag^+ and Se^{2-}.[40] The binding energies of the Ag 3d, Se 3d, C 1s and O 1s all indicated the formation of the Ag_2Se nanoparticles on the surface of LCNF. According to XPS, the microwave energy used in the preparation process did not have a significant impact on the surface chemistry or composition of the material. The microwave-assisted synthesis does not necessarily negate other differences in properties such as crystallite size, and morphology.

3.4. Mechanical properties of LCNF/Ag_2Se films

The mechanical properties of LCNF/Ag_2Se films are shown in Fig. 6. Fig. 6a displays the stress–strain curves of samples A50, A75, B50, and B75. Samples A75 and B75, which contain 75%

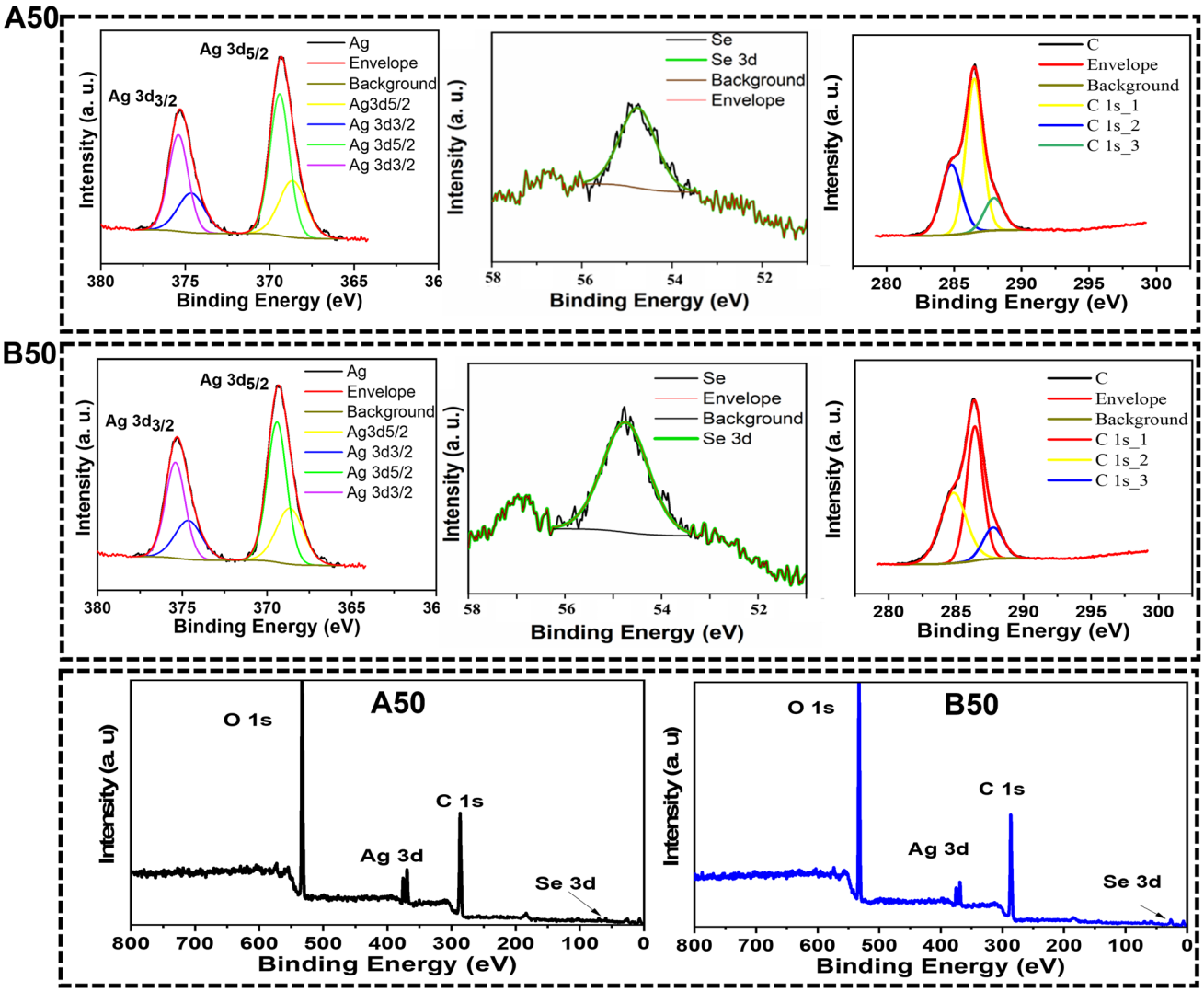

Fig. 5 XPS spectrum of LCNF/Ag_2Se composites for samples A50 and B50.

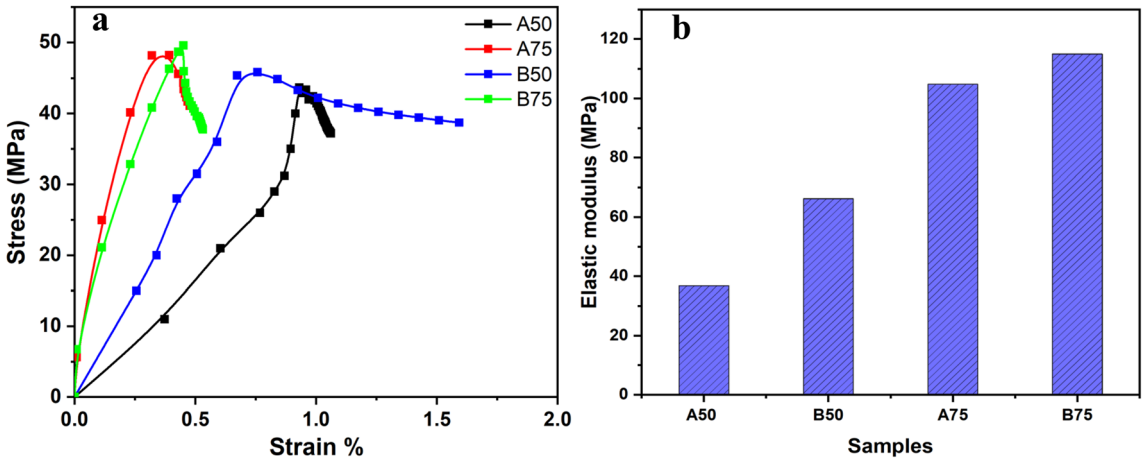

Fig. 6 (a) Stress–strain curves and (b) elastic modulus for different LCNF/Ag_2Se samples.

Ag_2Se, exhibit the highest stress values compared to A50 and B50. Additionally, the elastic modulus values (Fig. 6b) indicate that samples A75 and B75, both with 75% Ag_2Se, possess significantly higher modulus values compared to samples with lower Ag_2Se content. This suggests that a higher concentration of Ag_2Se nanoparticles contributes to enhanced stiffness and strength of the composite films. These results are crucial as they confirm that the incorporation of Ag_2Se nanoparticles significantly improves the mechanical properties of the films. The enhanced mechanical strength and stiffness are necessary for the application of these films in flexible thermoelectric devices, ensuring they can withstand mechanical stress and maintain performance over time.

3.5. Performance of the TE generators

Fig. 7 shows measured open-circuit voltage (V_{oc}) with temperature difference (ΔT) of 10, 20, 30, 40, and 50 K temperature difference between the hot and the cold sides of the circuit. The results demonstrate that the generated voltage increases with the ΔT (K). Specifically, the highest voltages recorded at a ΔT of 50 K were 18 mV, 21 mV, 19 mV, and 33 mV for samples A50, A70, B50, and B70, respectively (Fig. 7a and c). This indicates a direct correlation between ΔT and the thermoelectric voltage output, showcasing the efficiency of the LCNF/Ag_2Se composites in converting thermal gradients into electrical energy. This enhancement in voltage output in B50 and B70 samples is attributed to a more effective involvement of active materials in the power generation process facilitated by the microwave-assisted preparation. The Seebeck coefficient is a measure of the thermoelectric voltage generated between two points for a unit temperature difference between them. It is a key factor in determining the performance of LCNF/Ag_2Se TE. The definition can be expressed as

$$S = \frac{V_{oc}}{N \times \Delta T} \quad (2)$$

where S is the Seebeck coefficient and V_{oc} is the TE voltage, ΔT is the temperature difference, and N is the number of legs in the module. Fig. 6b displays the Seebeck coefficients of the flexible TE that were calculated from the single leg of LCNF/Ag_2Se TE. At a temperature difference of $\Delta T = 50$ K, the average Seebeck coefficients were found to be −60, −70, −63.3 and −110 μV K^{-1} for samples A50, A70, B50 and B70 respectively. Samples B50 and B70, which were prepared using microwave energy, demonstrated improved in Seebeck values when compared to samples A50 and A70, which were prepared without microwave energy. The data shows that B50 exhibited a higher Seebeck coefficient than A70 at 300 K. However, this trend reversed between 310 K and 340 K. The higher Seebeck coefficient at 300 K for B50 can be attributed to the optimized distribution and smaller size of Ag_2Se nanoparticles achieved through microwave-assisted synthesis, which enhances the thermoelectric properties by improving the electron transport pathways and reducing scattering. The microwave treatment likely results in a more uniform and densely packed structure, leading to a higher Seebeck coefficient at lower temperatures. Fig. 7c illustrates the open-circuit voltage of various LCNF/Ag_2Se samples at a temperature difference of 50 K.

Fig. 7d demonstrates a consistent voltage trend over 100 seconds, suggesting that within this time frame, the open-circuit voltage remains stable. This observation highlights the stability of the performance of the material within this specific timeframe. The observed stability in the LCNF/Ag_2Se open-circuit voltage over 100 seconds provides valuable insights into its temporal behavior as a thermoelectric material. It indicates that the performance of the material remains steady and consistent over an extended period. This stability suggests that the material exhibits consistent power generation capabilities, making it a reliable candidate for practical applications. The stability of the open-circuit voltage in LCNF/Ag_2Se has important implications for its potential use in various thermoelectric applications. It suggests that within the specified timeframe, the material maintains consistent power generation capabilities, making it suitable for applications such as thermoelectric generators (TEGs) and waste heat recovery systems. The I–V curves (Fig. 7e) reveal a consistent decrease in voltage with increasing current for all samples, indicating a correlation between electrical conductivity and thermoelectric efficiency.

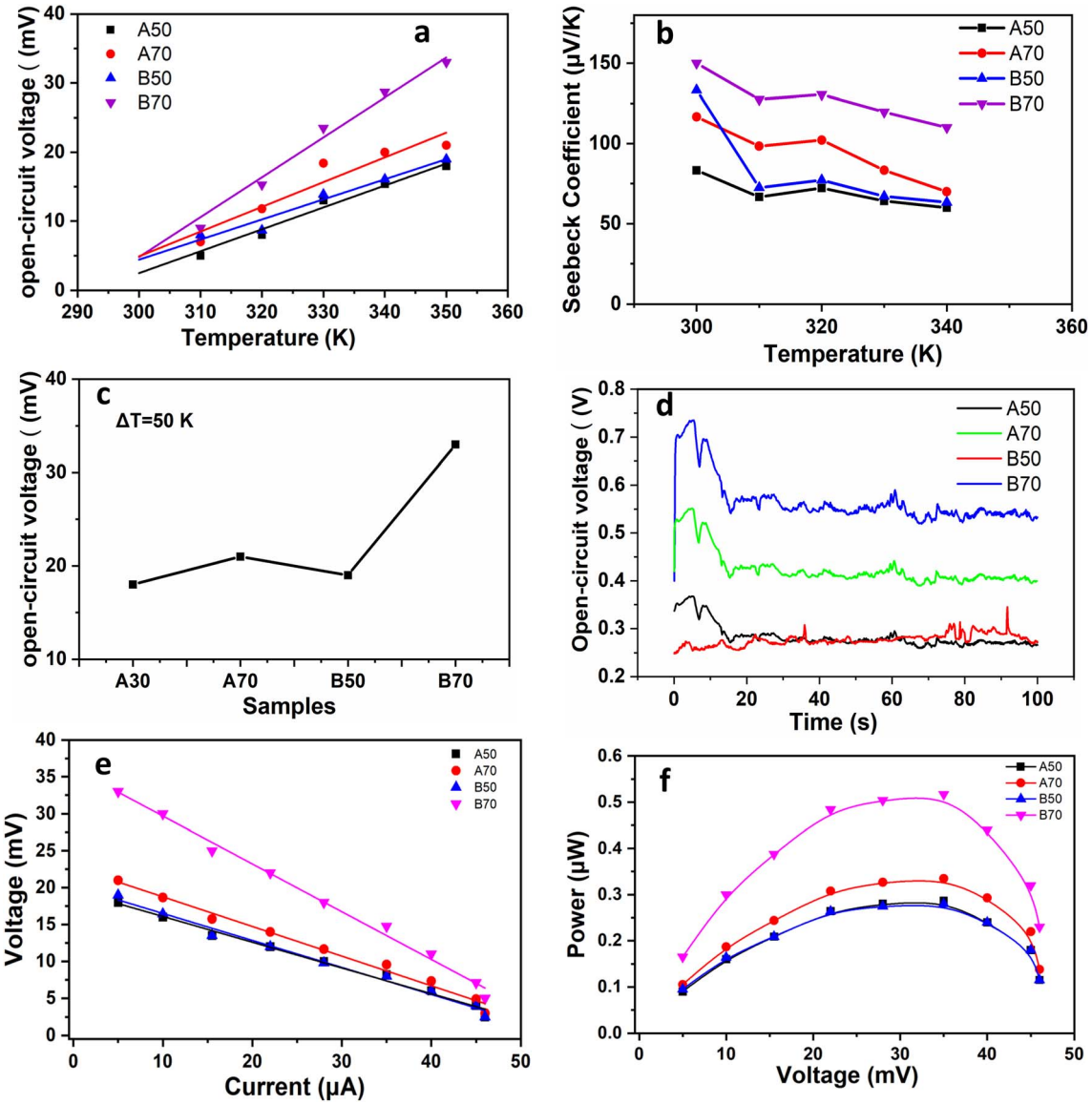

Fig. 7 LCNF/Ag_2Se thermoelectric performance tests: (a) open-circuit voltage at temperature differences of 10 to 50 K, (b) Seebeck coefficients for each sample, (c) open-circuit voltage at $\Delta T = 50$ K for all samples, (d) stability of open-circuit voltage for B50 over time, (e) voltage–current and (f) power-voltage at $\Delta T = 50$ K.

Notably, the B70 sample exhibits the highest voltage across the entire current range, suggesting superior conductivity and efficiency. Furthermore, Fig. 7f of the *P–V* curves illustrate the power output of each sample, with the B70 sample demonstrating the highest power output due to its optimized synthesis process and higher Ag_2Se content, making it a highly promising material for thermoelectric applications.

4. Conclusions

The successful synthesis of a flexible LCNF/Ag_2Se nanocomposite film, achieved through *in situ* synthesis with and without microwave energy assistance, demonstrated a significant advancement in thermoelectric material fabrication. Microwave energy played a crucial role in enhancing the thermoelectric properties of these films, notably increasing output voltages and Seebeck coefficients at temperature difference between the sides of the circuit. SEM and TEM analyses revealed a uniformly dispersed distribution of Ag_2Se within the LCNF nanofiber network in films with 50% and 70% Ag_2Se content, emphasizing the effectiveness of the fabrication process. The study demonstrated the potential of microwave assisted LCNF/Ag_2Se films as efficient and flexible materials for thermoelectric energy generation, especially in wearable and flexible electronics.

Data availability

The data that support the findings of this study are available from the corresponding author.

Author contributions

This manuscript was written with contributions from all authors, and the final version has been approved by all authors.

Conflicts of interest

No conflicts require declaration.

Acknowledgements

The authors acknowledge the financial support USDA Forest Service/US Endowment (21-00157), USDA Forest Service (22-DG-11083150-201), Louisiana Board of Regents [LEQSF(2020-23)-RD-B-02] and National Science Foundation (2120640).

References

1 M. Haras and T. Skotnicki, *Nano Energy*, 2018, **54**, 461–476.
2 X. Li, K. Cai, M. Gao, Y. Du and S. Shen, *Nano Energy*, 2021, **89**, 106309.
3 Y. Du, J. Xu, B. Paul and P. Eklund, *Appl. Mater. Today*, 2018, **12**, 366–388.
4 X. Li, Y. Lu, K. Cai, M. Gao, Y. Li, Z. Wang, M. Wu, P. Wei, W. Zhao, Y. Du and S. Shen, *Chem. Eng. J.*, 2022, **434**, 134739.
5 M. Zhu, X.-L. Shi, H. Wu, Q. Liu and Z.-G. Chen, *Chem. Eng. J.*, 2023, **475**, 146194.
6 D. Yang, X.-L. Shi, M. Li, M. Nisar, A. Mansoor, S. Chen, Y. Chen, F. Li, H. Ma, G. X. Liang, X. Zhang, W. Liu, P. Fan, Z. Zheng and Z.-G. Chen, *Nat. Commun.*, 2024, **15**, 923.
7 T. Wei, P. Qiu, K. Zhao, X. Shi and L. Chen, *Adv. Mater.*, 2023, **35**, 2110236.
8 R. Santhosh, S. Harish, R. Abinaya, S. Ponnusamy, H. Ikeda, J. Archana and M. Navaneethan, *CrystEngComm*, 2023, **25**, 3317–3327.
9 J. L. Blackburn, A. J. Ferguson, C. Cho and J. C. Grunlan, *Adv. Mater.*, 2018, **30**, 1704386.
10 D. Li, C. Luo, Y. Chen, D. Feng, Y. Gong, C. Pan and J. He, *ACS Appl. Energy Mater.*, 2019, **2**, 2427–2434.
11 M. Tonga, L. Wei, E. Wilusz, L. Korugic-Karasz, F. E. Karasz and P. M. Lahti, *Synth. Met.*, 2018, **239**, 51–58.
12 Y. Zhao, Y. Li, J. Qiao, S. Jiang, P. Mao, J. Qiu, S. Kang, J. Tan, K. Tai and C. Liu, *Carbon*, 2020, **170**, 191–198.
13 Z. Zhang, S. Wu, Y. Niu, J. Jiang and C. Wang, *J. Mater. Sci.: Mater. Electron.*, 2019, **30**, 5177–5184.
14 H. Wang, X. Liu, Z. Zhou, H. Wu, Y. Chen, B. Zhang, G. Wang, X. Zhou and G. Han, *Acta Mater.*, 2022, **223**, 117502.
15 K. Zhou, J. Chen, R. Zheng, X. Ke, T. Zhang, X. Shi and L. Chen, *Ceram. Int.*, 2016, **42**, 12490–12495.
16 R. Santhosh, R. Abinaya, J. Archana, S. Ponnusamy, S. Harish and M. Navaneethan, *J. Power Sources*, 2022, **525**, 231045.
17 Y. Ding, Y. Qiu, K. Cai, Q. Yao, S. Chen, L. Chen and J. He, *Nat. Commun.*, 2019, **10**, 841.
18 Y. Lu, Y. Liu, Y. Li and K. Cai, *Compos. Commun.*, 2021, **27**, 100895.
19 Z. Shen, S. Kwon, H. L. Lee, M. Toivakka and K. Oh, *Int. J. Biol. Macromol.*, 2022, **222**, 3001–3013.
20 D. Palaporn, W. Mongkolthanaruk, K. Faungnawakij, K. Kurosaki and S. Pinitsoontorn, *ACS Appl. Energy Mater.*, 2022, **5**, 3489–3501.
21 F. Jiao, A. Naderi, D. Zhao, J. Schlueter, M. Shahi, J. Sundström, H. Granberg, J. Edberg, U. Ail, J. Brill, T. Lindström, M. Berggren and X. Crispin, *J. Mater. Chem. A*, 2017, **5**, 16883–16888.
22 R. E. Abouzeid, R. Khiari, N. El-Wakil and A. Dufresne, *Biomacromolecules*, 2019, **20**, 573–597.
23 M. S. Koo, S.-Y. Lee and Q. Wu, *Energy Fuels*, 2022, **36**, 4479–4490.
24 M. Shayan, R. Abouzeid, W. Xu, T. Wu and Q. Wu, *J. Mater. Chem. A*, 2024, **12**, 2820–2829.
25 R. Abouzeid, M. Shayan, T. Wu, J. Gwon, T. A. Kärki and Q. Wu, *ACS Appl. Polym. Mater.*, 2023, **5**, 7009–7021.
26 B. Sadeghi, P. Sadeghi, Y. Marfavi, E. Kowsari, A. A. Zareiyazd and S. Ramakrishna, *J. Appl. Polym. Sci.*, 2022, **139**, 51673.
27 Q. Long, G. Jiang, J. Zhou, D. Zhao, P. Jia and S. Nie, *Nano Energy*, 2024, **120**, 109130.
28 J. Fang, D. Liu, D. Xu, Q. Wu, H. Li, Y. Li and N. Hu, *Research*, 2022, **2022**, 2022–9854342.
29 D. Lee, J. Gwon, R. Huang, D. H. Picha and Q. Wu, *Food Hydrocolloids*, 2024, **150**, 109743.
30 A. Najahi, Q. Tarrés, P. Mutjé, M. Delgado-Aguilar, J.-L. Putaux and S. Boufi, *Nanomaterials*, 2022, **13**, 126.
31 K. Liu, H. Du, T. Zheng, W. Liu, M. Zhang, H. Liu, X. Zhang and C. Si, *Green Chem.*, 2021, **23**, 9723–9746.
32 H. Cheng and J. Ouyang, *J. Phys. Chem. Lett.*, 2022, **13**, 10830–10842.
33 M. Zhu, C. Lu and L. Liu, *iScience*, 2023, **26**, 106718.
34 N. Dalton, R. P. Lynch, M. N. Collins and M. Culebras, *Int. J. Biol. Macromol.*, 2019, **121**, 472–479.
35 W. Mi, P. Qiu, T. Zhang, Y. Lv, X. Shi and L. Chen, *Appl. Phys. Lett.*, 2014, **104**, 133903.
36 R. Zuluaga, J. L. Putaux, J. Cruz, J. Vélez, I. Mondragon and P. Gañán, *Carbohydr. Polym.*, 2009, **76**, 51–59.
37 C. M. Ewulonu, X. Liu, M. Wu and Y. Huang, *Cellulose*, 2019, **26**, 4371–4389.
38 R. E. Abouzeid, R. Khiari, N. El-Wakil and A. Dufresne, *Biomacromolecules*, 2019, **20**, 573–597.
39 R. E. Abouzeid, R. Khiari, D. Beneventi and A. Dufresne, *Biomacromolecules*, 2018, **19**, 4442–4452.
40 S. Kumar, M. Tiadi, V. Trivedi, M. Battabyal and D. K. Satapathy, *ACS Appl. Energy Mater.*, 2023, **6**, 10457–10466.